AIAA 82-0403R

Ion Thruster Charge-Exchange Plasma Flow

M.R. Carruth Jr.,* S.B. Gabriel,† and S. Kitamura‡
Jet Propulsion Laboratory, California Institute of Technology, Pasadena, California

The electron bombardment ion thruster has been under development for a number of years, and during this time studies of the plasmas produced by the thrusters and their interactions with spacecraft have been evaluated based on available data. Because of diagnostic techniques used and facility effects, there is uncertainty as to the reliability of data from these early studies. This paper presents data on the flow of the charge-exchange plasma produced just downstream of the thruster's ion optics. The "end effect" of a cylindrical Langmuir probe is used to determine density and directed velocity of thruster charge-exchange ions. This technique allows some distinction between thruster ions and background facility ions. Results are compared with data obtained from a retarding potential analyzer Faraday cup where applicable.

Nomenclature

e = electronic unit of charge
ex = experimental value
E = directed kinetic energy
i = associated with ions
I = ion current for infinite cylindrical Langmuir probe
$I(0)$ = Langmuir probe current at $\theta = 0$
J = "end-effect" current for cylindrical Langmuir probe
K = Boltzmann's constant
L = cylindrical Langmuir probe length
M = mass of species
N = density of species
p = at cylindrical probe surface
R = cylindrical Langmuir probe radius
s = at a local spatial condition
S = parameter and function of σ
t = at target
T = temperature of species
U = directed velocity of flowing plasma ions
V = electric potential
X = function describing normalized end-effect peak structure
Z = axial distance from thruster optics plane
β = angle between Langmuir probe and ion beam axis
δ = $\exp(\delta^{-1})$ is characteristic nondimensional sheath radii
ϵ = ratio R/λ
η = normalized ion temperature
θ = angle between probe and plasma flow direction
λ = Debye length
μ = normalized angular half-width of ion curve peak
ν = dimensionless density parameter = 0.8
π = ratio of circumference of a circle to its diameter
ρ = r/R, where r is variable radial distance from center of the cylindrical Langmuir probe
σ = normalized probe length; defined in Eq. (14)
τ = dimensionless time criteria for probe length
Φ = angular full width at half maximum of ion current peak
ψ = dimensionless potential = $-eV/KT_e$

Presented as Paper 82-0403 at the AIAA 20th Aerospace Sciences Meeting, Orlando, Fla., Jan. 11-14, 1982; submitted Jan. 22, 1982; revision received June 8, 1982.

*Engineer. Present address: Marshall Space Flight Center, Ala. Member AIAA.
†Engineer, Electrical Power and Propulsion Section. Member AIAA.
‡Research Officer, Space Technology Group, National Aerospace Laboratory, Tokyo, Japan.

Introduction

THE electron bombardment ion thruster has been under development for a number of years. Ion thrusters are low-thrust devices that are capable of continuous operation for thousands of hours, have high specific impulse, and are very efficient. They therefore can have important applications in satellite station keeping, attitude control, orbit raising, and as primary propulsion for high-energy planetary missions.

A cutaway view of an ion thruster is shown in Fig. 1. Currently the ion thruster developed for space application utilize mercury as the propellant. Mercury is ionized in a discharge chamber and accelerated through ion optics which produces the thrust. An electron emitting neutralizer supplies an electron current to the ion beam to maintain spacecraft neutrality. A small amount, approximately 10%, of the mercury escapes from the discharge chamber through the optics without being ionized. Charge exchange interactions between these neutrals and the energetic ions downstream of the thruster optics form ions with only thermal energy. These ions leave the beam radially with a directed energy of from a few tenths to a few electron volts because of internal fields in the primary beam. These ions, with neutralizing electrons, constitute a charge-exchange plasma that can flow upstream around a spacecraft. It is very important to understand the thruster produced plasma environment in order to determine how it interacts with the spacecraft. The propagation of the charge-exchange plasma has been an area of uncertainty with several models developed to describe it.[1-7] The densities of the charge-exchange plasma predicted by these models at points upstream of an ion thruster vary by orders of magnitude.

It is very difficult to experimentally verify such models owing to the low directed energy of the ions and various effects produced by the test facility. Most experimental plasma characterization investigations to date have been performed with Langmuir probes and retarding potential analyzer (RPA) Faraday cups.[1,2] Such techniques are useful for determining plasma density, temperature, and directed energy when ion flow directions are known, but are relatively insensitive to measuring the direction of flow of the low-energy charge-exchange plasma. Such techniques cannot reliably distinguish ions which are produced by charge exchange between beam ions and neutrals which have previously encountered the chamber wall, i.e., facility produced ions.

The "end effect" of a cylindrical Langmuir probe has been used to determine the flow direction of the charge-exchange plasma from a 30-cm thruster at various locations relative to it.[8] The technique allows accurate determination of the flow direction at the probe location.

This paper presents data obtained by both an RPA and a cylindrical Langmuir probe, making use of the end effect. The use of the end effect to determine density and velocity of the

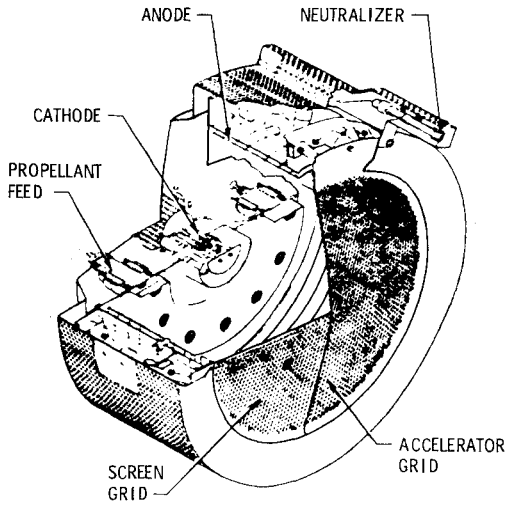

Fig. 1 Cutaway view of 30-cm *J*-series ion thruster.

flowing plasma as well as the flow direction is described. Comparison between velocity values obtained near the thruster by the RPA and the probe is made. To remain consistent with referenced papers on the end effect, CGS-ESU units are used.

Langmuir Probe "End Effect"

The ion current collected by an "infinite" cylindrical probe, i.e., where $L \gg R$, in a plasma under orbital motion limited (OML) conditions is given by[9]

$$I = 2N_i eURL(\sin^2\theta - 2eV_p/M_iU^2)^{1/2} \tag{1}$$

when $KT_i \ll -eV_p$ and $KT_i \ll \frac{1}{2}M_iU^2$. The current reaches a minimum at $\theta = 0$ and a maximum at $\theta = \pi/2$. However, the "end effect" can produce a large increase in current at $\theta = 0$ over that predicted by Eq. (1). The current I and the end-effect current, both as a function of θ, are illustrated in Fig. 2.

The end effect discussed in this paper was first reported by Bettinger and Chen to explain anomalous increases in ion current collected by a cylindrical Langmuir probe on the Explorer 17 satellite when it was aligned with the satellite's direction of motion.[10] The explanation for the increase in ion current is illustrated in Fig. 3. When the ion flow direction is at a large angle, θ, with respect to the probe axis, the impact parameter for ion collection is very small. When the probe is aligned with the plasma flow, a significant ion current can flow through the front of the sheath when $\lambda > R$. The ions experience the electric field along the probe and have a much greater likelihood of being collected. By obtaining the current as a function of the probe angle with respect to the plasma flow, a current peak can be obtained with an amplitude and half-width that are dependent on various plasma parameters and the ion flow velocity. The end effect can therefore be used for diagnostic purposes.

Hester and Sonin[11] and Sanmartin[12] pointed out that the Bettinger and Chen theory required a minimum probe length. The criteria for the probe to be of sufficient length for the Bettinger and Chen theory is

$$\tau = \frac{L}{\lambda}\frac{(KT_e/M_i)^{1/2}}{U} > 3 \tag{2}$$

Hester and Sonin and Sanmartin also pointed out that the Bettinger and Chen theory was based on various approximations but was approximately correct when Eq. (2) was fulfilled. Hester and Sonin presented a theory based on numerical calculations, for the condition of the probe being shorter than the above described minimum length. Sanmartin later presented a more complete, closed formula theory for the case of $\tau < 3$. Subsequent studies have indicated verification of Sanmartin's theory, at least in the study of energetic ions.[13,14]

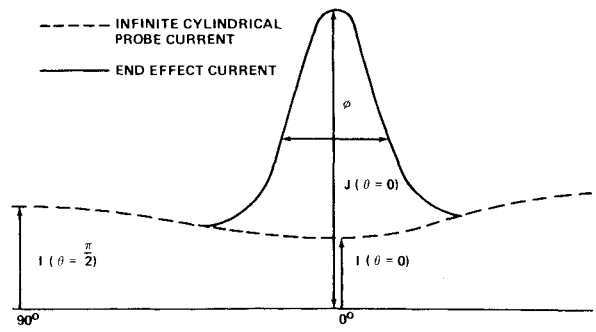

Fig. 2 Ion current peak illustrating *J*, ϕ, and *I*.

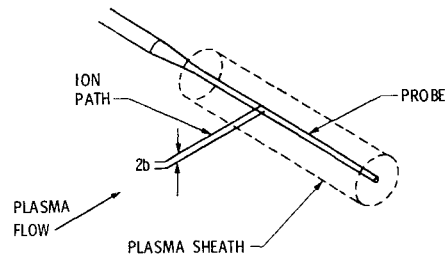

a) PROBE TRANSVERSE TO PLASMA FLOW

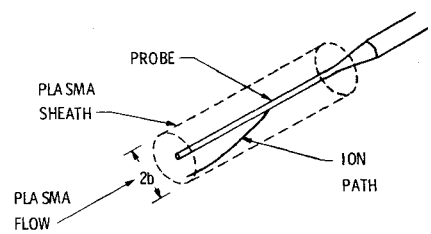

b) PROBE ALIGNED WITH PLASMA FLOW

Fig. 3 Illustration of end effect.

Sanmartin's "End-Effect" Theory—Conditions for Applicability

The Sanmartin analysis is based on a number of approximations; therefore there are certain conditions which must be fulfilled in order for the theory to be applied. They are[12]

$$U > (KT_e/M_i)^{1/2} \tag{3}$$

$$R < \lambda \ll L < 3\lambda U(M_i/KT_e)^{1/2} \tag{4}$$

$$KT_i \ll -eV_p < M_iU^2 \tag{5}$$

$$I \ll (-eV_p/KT_e) < (L/\lambda)^2 \tag{6}$$

These conditions place restrictions on the size of the cylindrical probe and the potential between it and the plasma for given plasma conditions. Previously obtained thruster plasma data were used to estimate limiting conditions on which to base probe size and probe potential so as to fulfill the above-stated conditions.

Sanmartin's analysis is for a single flowing plasma having ions with the same directed velocity. In this study it is applied to data obtained on the charge-exchange plasma. However, within the test chamber is neutral mercury which has been sputtered from the target and cryowall. Charge exchange interactions between these neutrals and beam ions will produce a low-energy "facility" charge-exchange plasma.

This will produce a background plasma with a general flow away from the sputter source. The question that arises is whether Sanmartin's theory can be applied in the cases where independent crossed flows exist or a background plasma exists along with a flowing plasma. The ion current collected due to the end effect is dependent on the sheath size, which is dependent on the total density at the probe position. Sanmartin found the electric field structure around the probe from Poisson's equation and assumed OML current collection. The field structure according to Sanmartin is[12]

$$\frac{\partial\psi}{\partial\rho} = \frac{-\psi\delta}{\rho} + \frac{\epsilon^2\nu(\rho^2-1)}{2\rho} \tag{7}$$

Integrating produces

$$\psi = -\psi_p\delta\ell n\rho + (\epsilon^2\nu/4)(\rho^2 - 2\ell n\rho - 1) + \psi_p \tag{8}$$

where

$$\delta = \ell n\psi_p + \ell n\delta - 2\ell n\epsilon - 0.3 \tag{9}$$

Since $\psi_p\delta \geq 1$ and varies slowly with density and $\epsilon \ll 1$, the first term dominates except for very large ρ. The Sanmartin theory is applicable for probe lengths such that $\tau < 3$. This is to say, it is short enough so that ions in the outer sheath are not collected. Therefore there is no need to consider very large ρ, especially with smaller and smaller τ. In general, for small τ the effects on the potential structure of the inner sheath due to a background density will be negligible if the background density is not considerably greater than the density of the flowing plasma. It has been previously shown that near the thruster the genuine charge-exchange plasma density is greater than facility plasma density.[2] Therefore, for the purposes of this study, the end-effect peak structure depends on the density of the flowing plasma the probe is aligned with.

End-Effect Peak Structure

Sanmartin derived an expression for the ion current peak structure. $X(\mu,\eta,S)$ is a direct representation of the peak structure, where[12,15]

$$X(\mu,\eta,S) = X_0^{\mu\eta} + SX_1^{\mu\eta} \tag{10}$$

and

$$\mu = U\sin\theta\,[M_i(\sigma^2-1)/(-eV_p\delta\ell n\sigma^2)]^{1/2} \tag{11}$$

$$\eta = 2KT_i(\sigma^2-1)/-eV_p\delta\ell n\sigma^2 \tag{12}$$

$$S = 2(1-\sigma^{-2})/\ell n\sigma^2 \tag{13}$$

$$\sigma\mathrm{erf}(\ell n\sigma)^{1/2} = L[-2eV_p\delta/(\pi U^2M_iR^2 + 2.4\pi N_iL^2R^2e^2)]^{1/2} \tag{14}$$

The exact expressions for $X_0^{\mu\eta}$ and $X_1^{\mu\eta}$ are such that integration within them can not be carried out. Limiting values can be found for the cases where $\eta \to 0$, the cold-ion case, and $\mu \to 0$, the value of $X(\mu,\eta,S)$ at $\theta = 0$. It can also be shown from Sanmartin's equations that $X_0^{\mu\eta}$ is always much greater than $SX_1^{\mu\eta}$. Therefore, from Eqs. (56) and (57) of Ref. 12,

$$X_0^{\mu 0} = (2/\pi)[\sin^{-1}\mu^{-1} + (\mu^2-1)^{1/2}/\mu^2] \tag{15}$$

$$X_0^{0\eta} = \mathrm{erf}\eta^{-1/2} + 2(\pi\eta)^{-1/2}\exp(-\eta^{-1}) - 2\eta^{-1}\mathrm{erfc}\eta^{-1/2} \tag{16}$$

Based on the anticipated range of charge-exchange plasma densities and flow velocities, $\sigma \gg 1$ and therefore $\eta \gg 1$. This will allow some simplifications. First,

$$\sigma\mathrm{erf}(\ell n\sigma)^{1/2} \approx \sigma \tag{17}$$

and

$$\mathrm{erf}\eta^{-1/2} \approx 2\eta^{-1/2}/\pi \tag{18}$$

and

$$\mathrm{erfc}(\eta^{-1/2}) \approx 1 - 2\eta^{-1/2}/\pi \tag{19}$$

Applying the above described approximations to Eqs. (61) and (65) of Ref. 12, for the peak current and half-width, respectively,

$$J(\theta=0) = \pi R^2\sigma^2N_ieU[4(-eV_p\delta\ell n\sigma^2)^{1/2}/(2\pi KT_i\sigma^2)^{1/2} + eV_p\delta\ell n\sigma^2/\sigma^2KT_i] \tag{20}$$

and

$$\phi = (16/\pi)(-eV_p\delta\ell n\sigma^2/U^2M_i\sigma^2)^{1/2} \times [4(-eV_p\delta\ell n\sigma^2/2\pi\sigma^2KT_i)^{1/2} + eV_p\delta\ell n\sigma^2/\sigma^2KT_i]^{-1} \tag{21}$$

Equations (20) and (21) relate N_i and U to J and ϕ, which are obtained directly from the end-effect peak. However, there is another unknown, T_i. Unlike other Langmuir probe techniques, the structure of the end-effect peak is dependent on T_i. The temperature inside the discharge chamber of the ion thruster is used as an approximate number for T_i. This value is about 500° K.[16] The charge-exchange plasma ions are created from neutral atoms leaking through the ion optics. Therefore they possess the thermal energy associated with the thruster's internal temperature since the mean free paths in the beam are very large, and the ions will not be involved in inelastic collisions which can change their thermal energy before being collected by the Langmuir probe. This, of course, assumes the ions flow as though from a point source. Any distribution of apparent sources causing nonparallel directed flow at the probe position will produce an effective temperature in excess of true random motion. Fortunately, also, J and Φ only vary as $T_i^{-1/2}$.

Notice in Fig. 2 that J in Sanmartin's theory includes the current I. There is a problem with determining the baseline from which to measure I and J because of the requirement to fulfill Eq. (5). Because of the low directed energy of the ions, V_p must be small. Therefore the electron current to the probe is nonzero and an uncertain amount. Also, the background facility ions are contributing to the ion current. Equation (1) indicates that at $\theta = 0$,

$$I = 2N_ieRL(-2eV_p/M_i)^{1/2} \tag{22}$$

Noting that the end-effect peak typically affects the ion current vs θ curve only at small θ, the curve at large θ can be extrapolated to $\theta = 0$ and $J - I$ determined. By systematically choosing the baseline, Eqs. (20-22) can be solved to determine N_i, U, and I.

Experimental Arrangement

A schematic diagram of the experimental arrangement is shown in Fig. 4. The vacuum chamber is 2.1 m in diameter and 4.6 m long, and is cryopumped by a liquid nitrogen (LN_2) cooled liner. A mercury ion thruster is placed at one end of the chamber such that the ion beam impinges on a frozen mercury target at the other end of the chamber. This target can be rotated through 90 deg, allowing the beam to strike the frozen mercury target or the end of the chamber. The use of a frozen mercury target reduces sputtering of the steel walls of the vacuum chamber. In addition to the cryopumping, the chamber is pumped by two 81-cm oil diffusion pumps (with LN_2 cooled baffles) providing a background pressure in the range $(1\text{-}6)\times 10^{-6}$ Torr with the thruster operating.

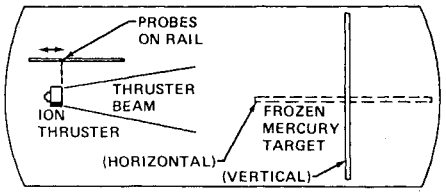

Fig. 4 Experimental arrangement; probes may move upstream or downstream of thrust plane.

The ion thruster used in these experiments is a 900 series, Hughes 30-cm mercury thruster with small hole accelerator grid (SHAG) optics. The ion beam output of the thruster is therefore equivalent to that from a *J*-series 30-cm ion thruster. The thruster is operated and throttled as recommended for a *J*-series thruster by NASA-LeRC.[19]

The thruster is not operated in a completely "floating" mode but to ensure effective neutralization by the hollow cathode neutralizer, the neutralizer is biased approximately 14 V negative with respect to ground. Using this arrangement, the neutralizer emission current can be made equal to the beam current. However, it should not be assumed that electrons from the tank walls do not contribute to neutralization. Complete neutralization can only be guaranteed and verified by running the system in a completely "floating" mode.

Two probes are used to characterize the charge-exchange plasma: a cylindrical Langmuir probe and an RPA probe. The Langmuir probe is made from tungsten wire, 0.13 mm in diameter, and has a length-to-diameter ratio of 79 to 1. The probe can be rotated about its midpoint from -90 to $+90$ deg, where 0 deg is defined as that position where the probe is perpendicular to the thruster beam axis. When the probe is at the -90 deg position, it is parallel to the thrust beam and pointed at the target end of the chamber, while at the $+90$ deg position it is pointed at the thruster end of the chamber. The probe is biased approximately 1 V negative of the plasma potential, which is found by changing the bias voltage until the peak current due to the end effect has disappeared. When this occurs the probe is at potential V_s. Probe cleaning is achieved by two methods: applications of a high-positive potential causing heating to white-hot temperatures (for a minute or so) caused by electron collection, and ion bombardment cleaning by application of a high-negative potential of approximately 1 kV.

The RPA probe is of a conventional design with two "grids" and a collector. Each grid is constructed of mesh with 50 wires/in., each wire being approximately 0.25 mm in diameter. The entrance grid is attached to the body of the probe and is isolated, allowing it to be biased to plasma potential. The collector is biased at -20 V to repel electrons and the retarding grid can be biased from 0 to $+40$ V. Ion energies are calculated by measuring the collected current with a picoammeter for different retarding grid potentials. The entrance grid is also used to measure the floating potential.

Both probes are mounted on a rail which was placed in the chamber so that it is parallel to the thruster beam axis. The probes are separated by 22.5 cm and are driven linearly along the rail using a motor drive. At each location, measurements are made of the cylindrical probe collected current vs angle, plasma and floating potentials, and ion energy spectrum.

Operating conditions for the thruster are beam current, 1 A; screen grid voltage, 1.1 kV; accelerator grid voltage, -0.35 kV; discharge voltage, 32 V; discharge current, 8.0 A; and propellant utilization efficiency, 0.95.

Facility Produced Ions

Facility produced effects have long been recognized as making reliable measurements of the charge-exchange plasma difficult.[1,2] One of the major difficulties is subtracting the facility produced plasma from measured signals to determine thruster charge-exchange plasma values. The beam strikes the target at the end of the chamber and neutral atoms are sputtered from the target. These atoms flow upstream and may be charge-exchange ionized in the beam. This produces low-energy ions which are difficult to distinguish from thruster charge-exchange ions, i.e., those ions which are produced by charge exchange between beam ions and neutrals escaping from the thruster's discharge chamber.

The end effect of a cylindrical Langmuir probe will produce increased ion current when the probe is aligned with a flowing plasma. If there are a number of flowing plasmas crossing at the probe's location, an ion current peak will be produced by each one as the probe is aligned with them. Depending on conditions, the end-effect peak may be only a few degrees wide. It is because of this angular sensitivity that the end effect was applied to the study of the ion thruster charge-exchange plasma.

In the original report by Carruth and Brady on the use of the end effect to study the ion thruster's charge-exchange plasma, several observations were made.[8] They are that the charge-exchange plasma possesses a definite directed flow; that the end-effect peak was only slightly affected by significant changes in background neutrals, indicating the peak is produced by thruster charge-exchange ions; and that the data indicated there were facility ions coming from the direction of the target. All indications were that the thruster charge-exchange plasma produced the observed end-effect peak independent of facility ions.

The data presented in this paper are, in some ways, different from that reported by Carruth and Brady. However, the experimental facility and apparatus are the same. In the earlier study the emphasis was on determining the charge-exchange plasma flow direction. This paper goes a step farther and determines the number density and velocity of the flowing ions. Therefore the cylindrical Langmuir probe length was modified to fulfill the requirements of Sanmartin's theory. Also, an RPA was added to provide data which could be compared with results obtained from the cylindrical Langmuir probe. The initial results from the RPA indicated directed energy of the charge-exchange ions of about 15 eV. This was much in excess of that expected based on a low T_e and potential variation across the beam.[17] It was determined that the ion thruster's neutralizer was not functioning properly and was consequently replaced. The directed energy of the charge-exchange ions dropped to just over 1 eV, as measured by the RPA, after the neutralizer was replaced.

A comparison is made between the data presented in this report and that presented in previous work by Carruth and Brady. The data are similar in that the flow directions at various probe locations indicate the charge-exchange plasma flows radially from the beam just downstream of the ion optics of the thruster and then expands outward so the flow directions turn both upstream and downstream. However, in the previous work, the width of the end-effect peaks were much less than obtained in this work. This indicates that the directed ion velocity was greater in the previous work. It is therefore possible that the neutralizer was functioning improperly when the previous data were acquired. Carruth and Brady reported energies of the flowing ions to be from 1 to 3 eV based on velocities obtained using the end-effect theory of Bettinger and Chen and Eq. (1). Because $E \alpha U^2$, an error of a factor from 2 to 3 can explain the considerable difference in energy determined from their calculations and that observed by the RPA before replacement of the thruster's neutralizer. Such an error may be caused by the fact that a "cold-ion" approximation of the end-effect theory was used.[11] Because of the reported low T_e in a 30-cm ion thruster beam, it is questionable that such an approximation is valid. In the previously reported work, the end-effect peak, even for far upstream position, did not change greatly when the chamber neutral mercury was significantly altered and only a single peak was observed. Also, there was evidence of a facility

plasma flow from the chamber target. Carruth and Brady concluded that the facility plasma ions coming from the target did not affect the peak and therefore the peak represented the thruster charge-exchange plasma.

The data presented in this paper indicate that for downstream positions, the end-effect peak increases from about 20 to 40% when the mercury target is moved from the horizontal to the vertical position, but for positions upstream of the thruster this change may be a factor of 2. Even more pronounced is the observation of two individual peaks for positions just upstream of the thruster with the magnitude of the small peak diminishing for positions farther upstream. Partial explanation for the difference between data presented here and that presented by Carruth and Brady lies in the consideration of the facility ions. Carruth and Brady considered the most important facility ions to be those produced from atoms sputtered from the target and flowing upstream. In so doing, they considered only one facility ion source. Figure 5, taken from another study, indicates that facility ion production peaks near the mercury target, where the neutral density is highest, and also near the thruster, where beam density is the highest.[18] Therefore, there are effectively two facility ion sources to consider. One is the facility ions created near the target and flowing upstream. These were observed by Carruth and Brady. The other is the facility ions created near the thruster. The sputtered mercury target atoms and, therefore, these facility ions have an initial upstream velocity of about 1 eV. If, in the case of Carruth and Brady, the radially directed charge-exchange ion velocity outside the beam was from 10 to 15 eV, the 1-eV initial velocity would have had minimal significance. However, in the case presented in this paper where the radially directed velocity is between 1 and 2 eV, the initial directed energy of an ion will have more significance in determining the velocity and flow direction at a given location. This can explain the resolution of two upstream peaks in data presented in this paper. Because of the facility ions' initial upstream direction, the peak at the largest cylindrical probe angle is expected to be produced by the facility ions. If this is true, then the major peak is facility ions and the small peak is produced by thruster charge-exchange ions. It is very difficult to distinguish for sure which of the peaks represent facility ions and which represent thruster charge-exchange ions. Also, the explanation presented here for the two peaks, which also explains the decrease in the large upstream peak caused by a significant decrease in mercury neutrals in the chamber, does not explain why Carruth and Brady did not observe a similar occurrence. More insight into the production of the two peaks and the effects of facility ions can be obtained by collecting data from a thruster operating in a different size facility.

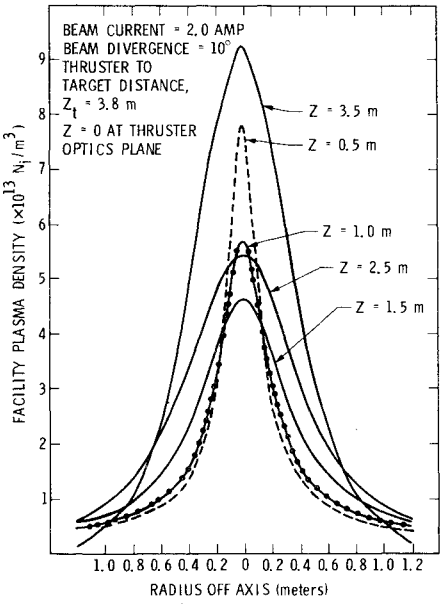

Fig. 5 Calculation of facility ion density (Ref. 18).

Data Analysis and Discussion

Method

An iteration method was conceptualized to allow for the undetermined baseline of the end-effect probe trace. In the experiment there are some causes which shift the probe trace up or down relative to zero net current. Besides thruster charge-exchange ions, low-energy facility ions can be present which will cause additional ion collection by the probe and shift the trace up. If the probe is not biased negatively enough to repel all electrons, the electron current to the probe will shift the trace down. The iteration method has made it possible to determine U and N_i even in those cases of unknown baselines since this method does not utilize the information of absolute values of the peak currents from the baseline but depends only on the shapes of the peak current profiles. Any effect which causes the probe trace to shift can be allowed for if it does not have strong dependence on the probe angle θ. It is also necessary to assume an ion temperature in this iterative method.

Sanmartin's theory can give the peak current profile $J(\theta)$ shown by the solid curve in Fig. 2, and the probe theory for an infinitely long probe can give the baseline current $I(0)$ shown by the dotted curve; this dotted curve can be found by extrapolation from large θ. Then, although profiles of $J(\theta)$ and $I(0)$ cannot be determined directly from the experimental trace, the difference of these two profiles, $J(\theta)-I(0)$, can be obtained. These profiles, $J(\theta)-I(0)$, contain enough information to solve Eqs. (20-22) and get N_i and U for an assumed ion temperature.

The idea in this method is to solve

$$J(\theta)-I(0)=J_{ex}(\theta) \tag{23}$$

Since $J(\theta)$ is a function of N_i, U, and θ, and $I(0)$ is a function of N_i, Eq. (23) can be solved to determine N_i and U by evaluating it at two different θ's because of the two unknowns. In fact it is evaluated at the peak $\theta=0$ and at the half angle $\theta=\Phi/2$ because the Sanmartin theory gives the explicit equations at these two angles.

Basically it may be possible to find the ion temperature as well as density and velocity if $J(\theta)$ is considered as a function of N_i, U, and T_i, and Eq. (23) is evaluated at three different θ's, or if a "best-fit" technique is used. However, this was not done because it would require more accurate data.

The real procedures start with finding the point $I(0)$ by extrapolation from the trace for large θ. Then, with the point $I(0)$ as the reference and the experimental peak profile, $J_{ex}(\theta)$, the true peak profile, $J(\theta)$, can be expressed by $J_{ex}(\theta)+I(0)$; the absolute value of $I(0)$ is unknown at this stage of the calculation.

In the iteration method with assumed ion temperature, the first step of the iteration assumes $I(0)=0$, which means that $J_{ex}(\theta)$ can be considered as the peak profile above the extrapolated curve in the first approximation. With this $J_{ex}(\theta)$ profile the peak current $J(0)$ and the half angle Φ can be determined in the first approximation. Using Eqs. (20) and (21) with $J(0)$ and Φ, solutions for U and N_i can be found.

Substituting N_i into Eq. (22) gives the baseline current $I(0)$ for the next step of the iteration. That is, the second approximation of the peak current profile can be obtained by adding this baseline current $I(0)$ to $J_{ex}(\theta)$. With this new peak current profile, new values for $J(0)$ and Φ can be found. By repeating these procedures until the new N_i is most nearly equal to the previous N_i, the final results for N_i and U can be found. Then the final, or real (in terms of the flowing ion

constituent), baseline current $I(0)$ can be determined. In the practical application of this iterative method there were probe traces which were affected by some angle-dependent effects. One of these effects was an asymmetrical ion current profile typical of the upstream regions. The ion currents for larger negative β were larger than those for large positive β. The larger ion currents are thought to be due to facility ions from the frozen mercury target because $\beta = -90$ deg corresponds to the direction of the target. In these cases, the iteration method was applied to the $+\beta$ half of the peak profile so that the facility ion flow is ignored and the density and speed of the thruster charge-exchange ions are obtained.

In some other cases where double peaks were observed, the ion current profiles were such that it was reasonable to assume that these profiles are composed of two kinds of ion flows. For these cases, it was assumed that the total ion current profile can be expressed by adding the two constituent ion currents. Then, if the current profile due to one of those ion flows is known by making reasonable assumptions, subtracting this current profile from the total will give the current profile due to the other ion flow. Such separation allows the iteration method to be applied to each flowing ion component.

Data Reduction

End-effect probe measurements were made for the two cases of the frozen mercury target in both horizontal and vertical positions. For each case, probe traces were taken at several locations along a line parallel to the thruster beam axis and 48 cm from it. Along this line, Z is defined such that positive Z corresponds to the downstream direction and negative Z to the upstream direction with $Z=0$ at the optical plane of the thruster. The same definition is used for the RPA positioning.

Figures 6 and 7 show typical traces of the end-effect probe for various locations. Curves for downstream positions are characterized by single ion current peaks near $\theta=0$. This means that the ions flow nearly radially from the beam to the tank wall. A two-peaked profile was obtained at $Z=-10$ and -20 cm. The far upstream current peaks are shifted to large negative β. This means that the ions flow nearly parallel to the ion beam axis. Although these illustrations are for the target horizontal, the same features were found also for the target vertical.

By examining how the currents and the angles at those peaks are changing with axial positions, it seems that primarily thruster charge-exchange ions give rise to single peaks for downstream regions and the small peaks for $Z=-10$ and -20 cm while facility ions give rise to the large peaks for $Z=-10$ and -20 cm, and single peaks for farther upstream regions.

This can be clearly seen in Figs. 8 and 9. Figure 8 shows a plot of the probe current peaks against axial positions and Fig. 9 shows a plot of probe angles for peak current against axial positions, where squares and circles denote the cases for horizontal targets and those for vertical targets, respectively. To distinguish thruster charge-exchange ions from facility ions, closed marks are used for the downstream single peaks and for the small peak of the double-peaked profiles, and open marks are used for the large peaks of the double-peaked profiles and for the upstream single peaks.

Since the magnitude of the peak current is an approximate indication of the ion density, Fig. 8 can illustrate how each constituent ion density changes with the axial position. The peak currents decrease rapidly from downstream to upstream (positive Z to negative Z) for the closed marked cases while

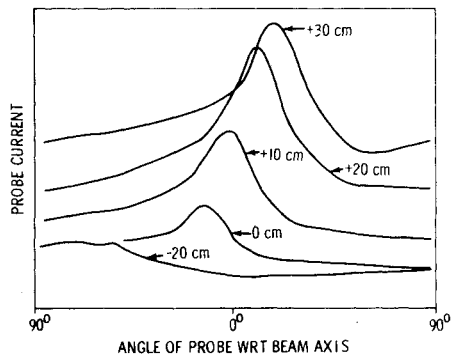

Fig. 6 Typical curves of probe current vs probe angle.

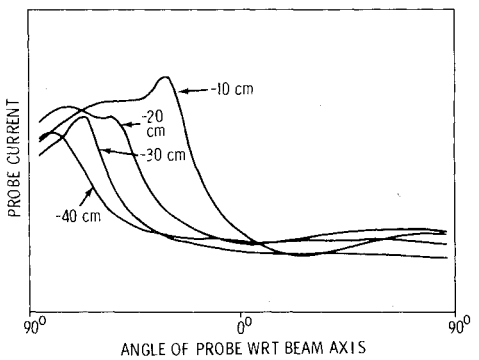

Fig. 7 Typical curves of probe currents vs probe angle upstream of thruster optics.

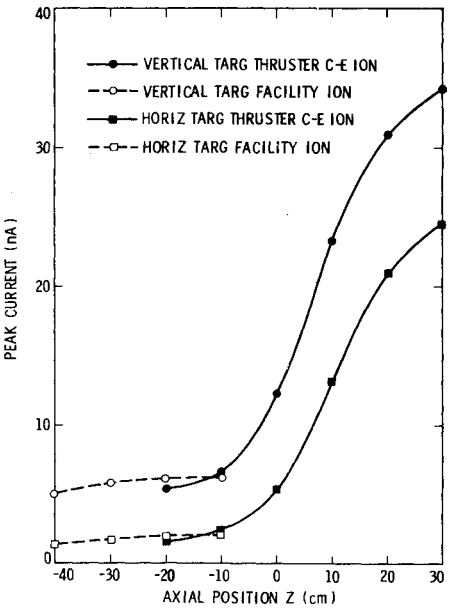

Fig. 8 Probe peak currents vs axial positions for horizontal and vertical positions of target.

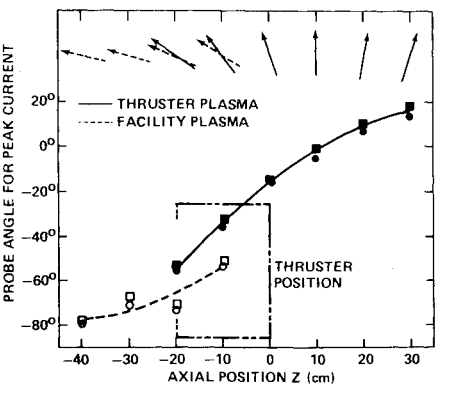

Fig. 9 Probe angle for peak current vs axial positions.

they are almost constant for open marked cases. This suggests that the former is due to thruster charge-exchange ions and that the latter is due to facility ions because each behaves as is expected from the following considerations.

Since facility ions are originally flowing from the direction of the target, their densities should be relatively constant over the short distance, say, less than 1 m. On the other hand, thruster charge-exchange ions are formed within a short distance downstream of the thruster. Thus they are more like a point source flow and moreover, they have to pass around the thruster to reach the upstream regions so that their densities should decrease rapidly with more negative positions.

Figure 9 shows that the facility ion flow occurs at more negative probe angles (toward the target) than the thruster charge-exchange ion flow. In Fig. 9, the arrows show the ion flow directions averaged for two cases of the target. They clearly illustrate that the thruster charge-exchange ions are mainly formed just downstream of the thruster and are spreading both radially and axially.

Figure 10 shows the end-effect probe trace at $Z=0$ cm for the horizontal target. Using this figure, a practical illustration of the iteration method will be given. The profile has a larger current for large negative β than for large positive β. The larger current of the left side is thought to be due to facility effects. Thus the right half of the peak has to be used to get information on the thruster charge-exchange ions. The line AA′ is drawn by the extrapolation from the current profile for large positive β. Then the peak currents from the line AA′ are used together with their angles as inputs to the iteration calculation, as shown by dots on the profile curve. After obtaining the results for N_i and U, the true baseline can be found using Eq. (22) and is shown as broken line BB′. In this case it is found that the true baseline BB′ is lower than the experimental zero-current line, which suggests that electron current to the probe dominates any current due to the presence of background ions.

Table 1 summarizes the results of end-effect measurements and RPA measurements. For downstream regions, where the ion densities are relatively high, the limit for the application of the Sanmartin theory becomes critical because the inequality

$$L<3\lambda U(M_i/KT_e)^{1/2} \tag{24}$$

must hold, and the right-hand side will become smaller for higher ion densities because of smaller Debye length λ. For these cases the iteration method shows poor convergence and an average of the closest N_i and U values to solve Eqs. (20-22) are used. The averaged values typically varied approximately 15%.

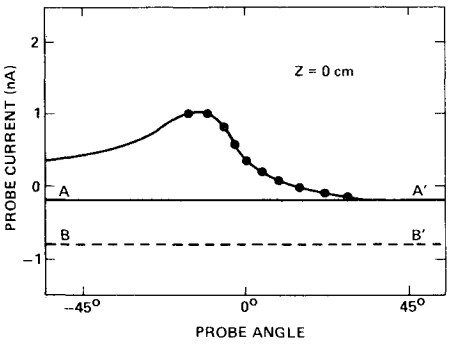

Fig. 10 Example of iteration method.

For $Z=-10$ and -20 cm, where the current profiles have double peaks, the assumption of current additivity is made. Two approaches are taken by the authors. One makes the assumption that the currents due to facility ions are almost the same for each upstream position. In this case the current profile of thruster charge-exchange ions, the small peak of the double peaks, is obtained by subtracting the current profile at $Z=-40$ cm from the profiles with double peaks. The normal method of current peak analysis is then applied to the resulting small peak. The other approach consists of extrapolating the larger peak of the $Z=-10$ and -20 cm curves and subtracting it from the current curve so as to obtain a symmetrical peak for the thruster charge-exchange plasma peak. The previously described method of current peak analysis is then applied. These two approaches gave density and velocity measurements which varied by as much as a factor of 3. Because of the relative size of the peaks to be separated, the procedure applied to separate them introduces error. The values given in Table 1 for $Z=-10$ and -20 cm are averages of values obtained by these two methods.

For $Z=-30$ and -40 cm, vertical target cases had higher peak current compared with horizontal cases. More facility ions are expected to be created for vertical cases because the direct collisions of beam ions and the frozen mercury target can create more mercury atoms to be charge exchanged in the facility. The difference between the ion profiles of the two cases indicate the increase in facility ions by the frozen mercury target. Because of the more volume source nature of the facility ions, the flow directions are not as unique as the thruster charge-exchange ions. Therefore the density and velocity values given in Table 1 for the two most upstream cases will have an additional error factor.

RPA measurements give the total ion energy relative to ground potential. By subtracting the plasma potential, V_s, from this total energy, the ion kinetic energy can be obtained. As previously mentioned, V_s is obtained by determining the voltage on the Langmuir probe at which the end-effect peak disappears. The kinetic energy obtained from the RPA is the radial component since the RPA is always pointed perpendicular to the thruster axis. Good agreement is obtained between the two diagnostics at positions where the charge-exchange plasma flow is radially outward from the beam axis.

Table 1 Ion number densities, directed ion energies, and plasma potential

Position Z, cm	Horizontal target N_i, ions/cm^3	Horizontal target E_i, eV	Vertical target N_i, ions/cm^3	Vertical target E_i, eV	$E_i=V_{RPA}-V_s$, eV	Plasma potential V_s, V
30	8×10^7	0.9	[a]	[a]	1.6-2.7	−0.4
20	7×10^7	0.9	8×10^7	1.0	1.6-2.6	−0.5
10	5×10^7	0.9	8×10^7	1.0	1.4-2.4	−0.4
0	3×10^7	0.9	4×10^7	0.9	1.9-2.1	−0.3
−10[b]	1×10^7	1.4	1×10^7	1.8	2.1	−0.5
−20[b]	5×10^6	1.4	5×10^6	1.8	[c]	−0.8
−30[d]	1×10^7	0.7	2×10^7	0.5	[c]	−1.2
−40[d]	1×10^7	0.5	2×10^7	0.5	[c]	−1.2

[a] Conditions of Eq. (24) violated. [b] Small peak, thought to be thruster charge-exchange ions. [c] Large angle between RPA and flow direction. [d] Thought to be primarily "facility" charge-exchange ions.

Concluding Remarks

The results of an experimental study to determine the flow direction, velocity, and density of the charge-exchange plasma produced by an ion thruster are presented in this paper. The end effect of a cylindrical Langmuir probe was used to determine these properties. An RPA was also utilized to acquire an independent value of ion velocity for comparison with values obtained from end-effect data collected by the Langmuir probe. Previous studies have verified Sanmartin's theory for plasma with ion directed energies from 20 eV to several hundred electron volts, but not for energies near 1.0 eV.[13,14] The agreement between the results obtained from the Langmuir probe data and the RPA data indicate the Sanmartin theory is valid for our plasma conditions. The agreement is quite good considering typical experimental error and the fact that Sanmartin's theory is derived for the ideal conditions of a Maxwellian ion population and a definite flow velocity and direction for the total ion population. We can expect to deviate some from this ideal condition because of the variation in potential in the beam at which charge-exchange ions are formed and the fact that the locations at which charge-exchange ions are created vary and can produce slightly differing flow directions at a position outside the beam. However, the RPA and Langmuir probe data and their agreement indicate that both the flow directions and energies are fairly unique.

The ion thruster beam strikes a frozen mercury target at the opposite end of the vacuum chamber. Since the target can be rotated in and out of the beam, the facility neutral population and, therefore, the facility plasma density can be significantly altered. Ion current peaks obtained with the Langmuir probe downstream of the ion thruster showed a 20-40% difference caused by rotation of the target. For positions upstream of the thruster the peak size alters significantly, approximately a factor of 2, as a function of target placement. This indicates that the downstream data obtained are primarily thruster charge-exchange ions while the upstream data are more strongly influenced by facility produced ions. Double peaks are resolved by the Langmuir probe end effect for upstream positions. Because of their flow directions and changes in magnitude as a function of position, the larger peak appears to be due to facility ions while the smaller peak appears representative of thruster charge-exchange ions. The smaller peak is therefore analyzed to obtain thruster charge-exchange plasma parameters.

The end effect of a cylindrical Langmuir probe may be concluded to be a useful technique for determining parameters associated with a low-velocity flowing plasma. It has proved useful in helping separate facility ions and true ion thruster charge-exchange ions. However, data from a different size facility are needed for better assessment of facility influence so that more accurate data on thruster charge-exchange ions can be obtained.

Acknowledgments

The research described in this paper was carried out at the Jet Propulsion Laboratory, California Institute of Technology, under NASA Contract NAS 7-100.

References

[1] Kaufman, H.R., "Charge-Exchange Plasma Generated by an Ion Thruster," NASA CR-135318, 1977.

[2] Komatsu, G. and Sellen, J.M. Jr., "Beam Efflux Measurements," NASA CR-135038, 1976.

[3] Poeschel, R.L. et al., "Extended Performance Solar Electric Propulsion Thrust System Study," Vol. 4, NASA CR-135281, 1977.

[4] Liemohn, H.B., Holze, D.H., Leavens, W.M., and Copeland, R.L., "Ion Thruster Plasma Dynamics Near High Voltage Surfaces on Spacecraft," AIAA Paper 79-2105, 1979.

[5] Parks, D.E. and Katz, I., "Spacecraft Generated Plasma Interaction with High-Voltage Solar Array," *Journal of Spacecraft and Rockets*, Vol. 16, No. 4, 1979, pp. 258-263.

[6] Robinson, R.S., Kaufman, H.R., and Winder, D.R., "Simulation of Charge Exchange Plasma Propagation Near an Ion Thruster Propelled Spacecraft," AIAA Paper 81-0744, 1981.

[7] Katz, I. et al., "Additional Application of the NASCAP Code," Vol. II, NASA CR-165350, 1981.

[8] Carruth, M.R. Jr. and Brady, M.E., "Measurement of Charge-Exchange Plasma Flow from an Ion Thruster," *Journal of Spacecraft and Rockets*, Vol. 18, Sept.-Oct. 1981, pp. 459-461.

[9] Mott-Smith, H.M. and Langmuir, I., "The Theory of Collectors in Gaseous Discharges," *Physical Review*, Vol. 28, 1926, pp. 727-762.

[10] Bettinger, R.T. and Chen, A.A., "An End-Effect Associated with Cylindrical Langmuir Probes Moving at Satellite Velocities," *Journal of Geophysical Research*, Vol. 73, No. 7, 1968, pp. 2513-2528.

[11] Hester, S.D. and Sonin, A.A., "Ion Temperature Sensitive End-Effect in Cylindrical Langmuir Probe Response at Ionospheric Satellite Conditions," *Physics of Fluids*, Vol. 13, May 1979, pp. 1265-1274.

[12] Sanmartin, J.R., "End-Effect in Langmuir Probe Response Under Ionospheric Satellite Conditions," *Physics of Fluids*, Vol. 15, June 1972, pp. 1134-1143.

[13] Fournier, G. and Pigache, D., "Transverse Ion Temperature in an Ionospheric Wind Tunnel," *Journal of Applied Physics*, Vol. 43, Nov. 1972, pp. 4548-4553.

[14] Mercure, H.P.E., "Ion Temperature Measurement in a Flowing Collisionless Plasma Using an End-Effect of Cylindrical Langmuir Probes," University of Toronto, Institute for Aerospace Studies, Report No. 202, July 1976.

[15] Sanmartin, J.R., "Ion-Temperature-Sensitive Effect in Transient Langmuir Probe Response," *Physics of Fluids*, Vol. 15, March 1972, pp. 391-401.

[16] Mirtich, M.J., "Thermal-Environment Testing of a 30-cm Engineering Model Thruster," AIAA Paper 76-1034, 1976.

[17] Komatsu, G.K., Cole, R.K., Hoffmaster, D.K., and Sellen, J.M. Jr., "Charge-Exchange Ion Formation and Motion in Mercury Ion Engine Thrust Beams," AIAA Paper 75-428, 1975.

[18] Carruth, M.R. Jr., "Facility Produced Charge-Exchange Ions," *Experimental and Analytical Evaluation of Ion Thruster/Spacecraft Interactions*, JPL Publication edited by M.R. Carruth, 80-92, 1980.

[19] NASA Lewis Research Center, "30 Centimeter Ion Thruster Subsystem Design Manual," NASA TM-79191, 1979.